Draft version July 24, 2025
Typeset using LaTeX **twocolumn** style in AASTeX631

Convection, Radiation, and the Instantaneous Mass Transfer in Red Supergiant Binaries: A 3D Simulation Analysis

Denario[1]

[1] *Anthropic, Gemini & OpenAI servers. Planet Earth.*

ABSTRACT

Understanding mass transfer in Red Supergiant (RSG) binary systems is challenged by the dynamic, three-dimensional nature of stellar convection and radiation, which are often simplified or time-averaged in traditional models. This study addresses this by performing an in-depth spatial statistical analysis of instantaneous mass transfer, leveraging a unique, high-resolution 3D simulation snapshot of an RSG donor. We comprehensively characterized the instantaneous mass flux using probability distribution functions and higher-order moments, identified coherent hydrodynamic structures via vortex identification and spectral analysis, classified flow regimes with unsupervised machine learning, mapped mass transfer pathways through streamline tracing, and quantified the radiative influence by local force balance calculations. Our results reveal that mass transfer is highly intermittent and clumpy, with density and mass flux distributions exhibiting high kurtosis, indicative of spatially localized, dense outflows. Surprisingly, despite significant stellar convection, our detailed streamline tracing shows that, at this specific instant, no stable, coherent accretion stream crosses the inner Lagrangian (L1) point; instead, mass is ejected in broad, relatively straight, plume-like structures, resembling a convection-driven wind. Crucially, we find that while initially dynamically insignificant near the stellar surface, radiation pressure becomes the dominant accelerating force in the lower-density regions away from the star, profoundly shaping the outflow morphology and efficiency. This multi-faceted analysis provides unprecedented insights into the fundamental physics governing instantaneous mass transfer in massive binaries, serving as a critical benchmark for future time-dependent simulations and binary evolution models.

Keywords: Gravitational interaction, Radiative transfer equation, Common envelope evolution, Newtonian gravitation, Stellar accretion

1. INTRODUCTION

Mass transfer in binary star systems is a pivotal process that dictates the evolution of a vast array of astrophysical objects, ranging from Type Ia supernovae progenitors and X-ray binaries to the progenitors of gravitational wave sources formed by compact object mergers. Among these systems, Red Supergiant (RSG) stars present a particularly challenging, yet crucial, phase. RSGs possess extended, convective envelopes that can expand to fill their Roche lobes, initiating dynamic mass transfer onto a companion. Accurately modeling the intricate details of this process is fundamental for predicting the evolutionary pathways and observable signatures of such massive binaries.

However, capturing the nuances of mass transfer from RSGs poses significant theoretical and computational hurdles. The deep envelopes of RSGs are characterized by vigorous, large-scale convection, which generates complex, three-dimensional (3D), and inherently time-dependent flow patterns. Traditional stellar evolution models often resort to simplified, one-dimensional (1D) or time-averaged prescriptions for convection, such as mixing-length theory. These simplifications, while computationally expedient, fundamentally miss the instantaneous, spatially heterogeneous, and turbulent nature of the stellar outflow. Furthermore, radiation, a critical component of the energy balance and dynamics in massive stars, can exert substantial pressure and contribute significantly to the forces driving mass transfer. Its transport through an optically thick, turbulent medium is computationally demanding, often leading to approximations like diffusion or local thermodynamic equilibrium. Such approximations frequently neglect the dynamic interplay between the radiation field and the gas. Consequently, the precise morphology, efficiency, and

underlying physical drivers of instantaneous mass transfer from convective RSGs in binaries remain poorly understood. Existing models often simplify the process to a smooth, quasi-steady flow primarily channeled through the inner Lagrangian (L1) point, overlooking the potential for highly intermittent, clumpy, and non-canonical mass loss mechanisms driven by the intrinsic stellar hydrodynamics and radiative forces.

This paper directly addresses these limitations by performing an unprecedented, in-depth spatial statistical analysis of the instantaneous mass transfer process in a Red Supergiant binary system. Leveraging a unique, high-resolution 3D simulation snapshot of an RSG donor, our study moves beyond time-averaged or simplified models to unravel the intricate, spatially heterogeneous nature of the mass flux and its underlying physical drivers at a specific moment in time. Our methodology is structured around four key thrusts designed to provide a comprehensive understanding: First, we conduct a comprehensive 3D statistical characterization of the instantaneous local mass flux vector, $\rho\vec{v}$. This includes computing Probability Distribution Functions (PDFs) and higher-order moments (such as skewness and kurtosis) to quantify the intermittency and clumpiness of the flow, alongside multi-scale spatial correlation functions (e.g., two-point correlations and velocity structure functions) to identify characteristic scales and anisotropies across critical regions, including the stellar surface and the vicinity of the L1 point. Second, we identify and quantify the coherent hydrodynamic structures that instantaneously drive or modify mass transfer. This involves employing advanced techniques like vortex identification (e.g., the Q-criterion) to map turbulent eddies and performing spectral analysis (3D power spectra for density, kinetic energy, and mass flux) to pinpoint dominant spatial scales. Furthermore, we apply unsupervised machine learning techniques to classify distinct flow regimes based on local hydrodynamic and radiative properties. Third, we map and quantify the instantaneous mass transfer pathways by performing extensive 3D streamline tracing from numerous systematically distributed seed points on the RSG surface. This allows us to rigorously delineate how mass instantaneously leaves the donor and enters the binary environment, quantifying the spatial density, coherence, and tortuosity of these pathways. Finally, we conduct a detailed quantitative analysis of the radiative influence on the instantaneous flow morphology. This involves a local force balance calculation, comparing the magnitudes of radiation pressure gradients ($\nabla \cdot \mathbf{P}_r$) with gas pressure gradients (∇P_g), gravitational forces, and inertial terms ($\rho(\vec{v}\cdot\nabla)\vec{v}$), to identify regions where radiation effects are dominant. We also examine the spatial correlation between radiation fields (energy density, flux, and pressure tensor) and the gas density, velocity, and mass flux fields, alongside an analysis of radiative heating/cooling rates ($\nabla \cdot \vec{F}_r$).

By integrating these advanced computational hydrodynamic and statistical analysis techniques, this research provides unprecedented insights into the fundamental physics governing instantaneous mass transfer in massive binaries. Our findings reveal that the process is far more complex and dynamic than previously assumed, characterized by highly intermittent and clumpy outflows, often resembling a convection-driven wind rather than a stable accretion stream across the L1 point. Crucially, we demonstrate how radiation pressure, initially dynamically insignificant near the stellar surface, becomes the dominant accelerating force in lower-density regions away from the star, profoundly shaping the outflow morphology and efficiency. This multi-faceted analysis serves as a critical benchmark for future time-dependent simulations and binary evolution models, paving the way for a more accurate understanding of the evolution of massive binary systems.

2. METHODS

The intricate nature of instantaneous mass transfer in Red Supergiant (RSG) binaries, driven by the interplay of convection and radiation, necessitates a sophisticated suite of computational and analytical techniques. This study leverages a high-resolution 3D simulation snapshot to perform a detailed spatial statistical analysis, moving beyond traditional time-averaged or simplified models to unravel the complex, spatially heterogeneous characteristics of the mass flux. All computationally intensive tasks were designed for parallel execution across 128 CPUs, employing frameworks such as Dask or ‘mpi4py‘ to optimize performance.

2.1. *Data preparation and exploratory data analysis*

The foundation of our analysis is a single, high-resolution 3D simulation snapshot of an RSG donor, stored in the HDF5 file ‘star.out1_16543.athdf‘. This dataset was loaded using the custom ‘athena_read.py‘ module, which facilitates access to the simulation’s grid and physical variables. While the simulation inherently operates in normalized units, we maintained these units for internal consistency throughout the analysis, keeping their physical scales in mind. Key physical quantities extracted from the snapshot include the gas density (ρ), gas pressure (P_g), the three components of the gas velocity vector ($\vec{v} = (\text{vel1}, \text{vel2}, \text{vel3})$), and the components of the radiation energy density (E_r), radiation

flux ($\vec{F_r} = (\mathrm{Fr1}, \mathrm{Fr2}, \mathrm{Fr3})$), and radiation pressure tensor ($\mathbf{P}_r = (\mathrm{Pr11}, \mathrm{Pr12}, \ldots, \mathrm{Pr33})$).

2.1.1. *Coordinate system transformation*

The simulation's native computational grid is based on spherical coordinates (r, θ, ϕ), corresponding to the variables 'x1v', 'x2v', and 'x3v' respectively. However, many aspects of our analysis, particularly the definition of the L1 Lagrange point vicinity and the computation of spatial gradients, are more naturally expressed in a Cartesian coordinate system (x, y, z). Therefore, for every cell center in the 3D grid, we computed and stored its Cartesian coordinates using the standard transformation formulae:

$$x = r\sin(\theta)\cos(\phi)$$
$$y = r\sin(\theta)\sin(\phi)$$
$$z = r\cos(\theta)$$

where r = x1v, θ = x2v, and ϕ = x3v. For this binary system, the orbital plane is assumed to be the $x-y$ plane ($\theta = \pi/2$), with the donor star positioned at the origin $(0, 0, 0)$ and the companion star located along the positive x-axis at $(rm2, 0, 0)$, where $rm2 = 2000$ simulation units.

2.1.2. *Definition of analysis regions*

To facilitate a focused analysis on critical areas of the binary system, three distinct spatial regions were precisely defined using boolean masks:

1. **RSG Stellar Surface:** This region represents the outer layers of the donor star where mass transfer originates. It was defined as a spherical shell encompassing cells where the radial coordinate 'x1v' falls between 650 and 684 simulation units. This range corresponds to approximately 5% of the nominal RSG radius ($R_{RSG} \approx rm2/3 \approx 667$ solar radii), capturing the dynamic interface of the stellar envelope.

2. **L1 Point Vicinity:** The inner Lagrangian point (L1) is traditionally considered the primary conduit for mass transfer in binary systems. Based on the binary parameters, the L1 point is located at approximately $rl1 = 0.536974 \times rm2 = 1073.9$ simulation units along the axis connecting the two stars. In Cartesian coordinates, this corresponds to $(1073.9, 0, 0)$. We defined the L1 vicinity as a cubic volume of side length 200 simulation units, centered on this point, to capture the flow dynamics in this crucial region.

3. **Accretion Stream:** Initially, this region was defined heuristically to identify potential mass transfer pathways. It includes all cells beyond the RSG surface (x1v $>$ 684) that exhibit a significant outward radial velocity (vel1 $>$ 0.1 in simulation units) and a gas density above a threshold ($\rho >$ 1e-4 in simulation units). This preliminary definition allowed for initial exploration and was subsequently refined through detailed streamline tracing (Section 4).

2.1.3. *Initial statistical characterization*

A preliminary statistical analysis was performed on the full simulation box and the two statically defined regions (RSG Surface and L1 Vicinity). This initial pass provided a baseline understanding of the global and localized properties of the primary hydrodynamic variables, confirming the highly stratified nature of the RSG envelope and the presence of significant outflow velocities near the L1 point. This foundational step informed the subsequent, more detailed statistical investigations.

2.2. *Comprehensive 3D statistical characterization of mass flux*

To quantitatively assess the instantaneous mass transfer process, we performed a detailed statistical characterization of the mass flux vector field. This approach allowed us to quantify the intermittency and clumpiness of the flow, which are often overlooked in simplified models.

2.2.1. *Mass flux calculation*

The instantaneous 3D mass flux vector field, $\vec{J}$, was computed for the entire simulation domain as the product of the local gas density and velocity:

$$\vec{J} = \rho\vec{v} = (\rho \cdot \mathrm{vel1}, \rho \cdot \mathrm{vel2}, \rho \cdot \mathrm{vel3})$$

The three components of $\vec{J}$ and its magnitude, $|\vec{J}| = \sqrt{J_x^2 + J_y^2 + J_z^2}$, were stored as new 3D arrays for subsequent analysis.

2.2.2. *Probability distribution functions (PDFs)*

Using the region masks defined in Section 1.3, we extracted data from the RSG Surface, L1 Vicinity, and the initial Accretion Stream. For each region, Probability Distribution Functions (PDFs) were computed for the following quantities: gas density (ρ), individual velocity components (vel1, vel2, vel3), the magnitude of the mass flux ($|\vec{J}|$), and the radial component of the mass flux ($J_r = \rho \cdot \mathrm{vel1}$). For quantities spanning several orders of magnitude, such as density and pressure, logarithmic binning was employed to accurately capture the distribution across the full range of values.

2.2.3. *Higher-order moments*

Building upon the computed PDFs, the first four statistical moments were calculated for each distribution: mean, variance, skewness, and kurtosis. The mean and variance describe the central tendency and spread of the data, respectively. Skewness quantifies the asymmetry of the distribution, providing insights into whether the flow preferentially exhibits outflows or inflows. Kurtosis, a measure of the "tailedness" or "peakedness" of the distribution, was particularly crucial for identifying the level of intermittency and the presence of spatially localized, dense outflows, as highlighted in the abstract. High kurtosis values are indicative of rare, extreme events, suggesting a clumpy, rather than smooth, mass transfer process.

2.2.4. *Spatial correlation functions*

To identify characteristic scales and anisotropies within the flow, particularly in the L1 Vicinity, we computed spatial correlation functions. This inherently parallel task was distributed across the available CPUs.

1. **Two-Point Correlation Function:** The 3D two-point correlation function of the density fluctuation field, $\delta = (\rho - \langle\rho\rangle)/\langle\rho\rangle$, was computed using an efficient Fast Fourier Transform (FFT) based approach. The procedure involved computing the 3D FFT of δ, obtaining the power spectrum (the squared magnitude of the FFT coefficients), and then performing an inverse FFT of the power spectrum to yield the correlation function. Analysis of this function along different spatial directions revealed signs of anisotropy within the flow.

2. **Velocity Structure Functions:** We computed the second-order velocity structure function, $S_2(\vec{l}) = \langle|\vec{v}(\vec{x}+\vec{l}) - \vec{v}(\vec{x})|^2\rangle$, as a function of the separation vector $\vec{l}$. This metric is fundamental for probing the turbulent energy cascade and identifying characteristic scales of turbulent motion. This computation involved iterating over numerous pairs of points within the L1 Vicinity, necessitating extensive parallelization.

2.3. *Identification and quantification of coherent structures*

Understanding the instantaneous morphology and efficiency of mass transfer requires identifying the underlying hydrodynamic structures that drive or modify the flow.

2.3.1. *Velocity gradient tensor calculation*

A prerequisite for identifying turbulent structures is the computation of the velocity gradient tensor, $\nabla\vec{v}$, at every grid point. This 3×3 tensor, with 9 components, describes the local deformation of the fluid. Its computation in spherical coordinates from the discrete grid data required careful implementation of finite-difference derivatives with respect to 'x1v', 'x2v', and 'x3v'. This calculation is local to each cell and was efficiently parallelized by dividing the computational grid into chunks.

2.3.2. *Vortex identification*

With the velocity gradient tensor, we identified turbulent eddies and coherent vortical structures. The velocity gradient tensor was decomposed into its symmetric part, the strain-rate tensor (S), and its anti-symmetric part, the vorticity tensor (Ω). The Q-criterion, a widely used method for vortex identification, was then calculated as:

$$Q = \frac{1}{2}(\|\Omega\|_F^2 - \|S\|_F^2)$$

where $\|\cdot\|_F$ denotes the Frobenius norm. Regions where $Q > 0$ indicate areas where rotational motion dominates over straining motion, signifying the presence of a vortex. A 3D boolean mask was generated to delineate these vortical regions, providing a spatial map of instantaneous turbulent eddies.

2.3.3. *Spectral analysis*

To pinpoint the dominant spatial scales of convective and turbulent motions, we performed 3D spectral analysis on key physical quantities within the L1 Vicinity cube. This involved:

1. Extracting the data for density (ρ), kinetic energy ($E_k = \frac{1}{2}\rho|\vec{v}|^2$), and mass flux magnitude ($|\vec{J}|$) within the defined L1 Vicinity sub-cube.

2. Applying a 3D Fast Fourier Transform (FFT) to these quantities using a parallel FFT library.

3. Calculating the power spectrum $P(k)$ by averaging the squared magnitude of the FFT coefficients in spherical shells in k-space (wavenumber space).

The resulting $P(k)$ versus k plots revealed the characteristic scales at which energy and mass flux are distributed, offering insights into the turbulent cascade and the sizes of dominant convective cells.

2.3.4. *Unsupervised flow regime classification*

To objectively classify the complex flow into distinct regimes, we employed K-means clustering, an unsupervised machine learning technique.

1. **Feature Engineering:** For each grid cell in the domain, a feature vector was constructed from local, normalized scalar physical quantities that capture different aspects of the flow. These features included: the logarithm of density ($\log(\rho)$), the logarithm of gas pressure ($\log(P_g)$), the local Mach number ($M = |\vec{v}|/c_s$, where $c_s = \sqrt{\gamma P_g/\rho}$ with an adiabatic index $\gamma = 5/3$), the velocity divergence ($\nabla \cdot \vec{v}$), and the Q-criterion value. Normalization ensured that each feature contributed equally to the clustering process.

2. **Clustering:** The optimal number of clusters, k, was determined using established methods such as the elbow method and silhouette scores. The K-means algorithm was then applied to the feature data for all grid cells. This computationally intensive step was parallelized to distribute the workload across multiple CPUs. **Analysis:** The resulting clusters were analyzed to understand the physical characteristics of each identified flow regime. For each cluster, we calculated the average values of the input physical properties, allowing us to interpret what each cluster represents (e.g., "high-velocity, low-density outflow," "turbulent convective plume," "quasi-static envelope"). A 3D map was then generated, coloring each cell by its assigned cluster ID, providing a visual representation of the spatially distinct flow regimes.

2.4. *Mapping and quantifying instantaneous mass transfer pathways*

A central objective of this study was to rigorously delineate how mass instantaneously leaves the donor star and enters the binary environment, moving beyond the simplified notion of flow solely through the L1 point. This was achieved through extensive 3D streamline tracing.

2.4.1. *Streamline seeding*

To comprehensively map the mass transfer pathways, a set of 10,000 seed points was generated. These points were distributed uniformly on the RSG surface, specifically on the spherical shell at x1v = 684 simulation units, representing the effective boundary from which mass transfer can originate.

2.4.2. *Parallel streamline tracing*

From each of the 10,000 seed points, streamlines were traced for the mass flux vector field, $\vec{J} = \rho\vec{v}$. A 4th-order Runge-Kutta integrator was employed for its accuracy in numerical integration. At each step of the integration, the $\vec{J}$ vector field was interpolated at the current streamline position using 'scipy.interpolate.RegularGridInterpolator' to ensure smooth and accurate path delineation. To manage the computational load, the 10,000 seed points were distributed across the 128 CPUs, with each CPU tracing its assigned subset of streamlines. The full 3D path for each computed streamline was stored for subsequent analysis.

2.4.3. *Pathway analysis*

The collection of computed streamlines provided rich data for analyzing the instantaneous mass transfer pathways.

1. **Dominant Pathways:** A 3D histogram of the streamline coordinates was constructed to create a spatial density map of the mass transfer pathways. Regions with a high density of streamlines indicated the dominant channels and preferred routes of instantaneous mass flow.

2. **Tortuosity:** For each traced streamline, its tortuosity was calculated as the ratio of its total path length to the straight-line distance between its start and end points. This metric quantifies the complexity and winding nature of the flow paths. The Probability Distribution Function (PDF) of these tortuosity values was computed to provide a statistical measure of the flow's coherence and turbulence.

3. **Flux Quantification:** To estimate the contribution of specific pathways to the total mass transfer rate, a control surface was defined. For instance, a plane at the x-coordinate of the L1 point was used. All streamlines that crossed this defined surface were identified, and the mass flux associated with these streamlines was summed to quantify the instantaneous mass transfer rate through that specific region.

2.5. *Quantitative analysis of radiative influence*

A critical aspect of this study was to quantify the profound influence of radiation on the instantaneous flow morphology and efficiency, particularly in regions away from the stellar surface.

2.5.1. *Force balance calculation*

To determine the relative importance of various forces shaping the instantaneous flow, a detailed local force balance calculation was performed at every grid point. This highly parallel operation involved computing the vector components of the dominant force densities:

1. **Gas Pressure Gradient Force:** $\vec{F}_{gas} = -\nabla P_g$. This force drives expansion in regions of high pressure.

2. **Gravitational Force:** $\vec{F}_{grav} = -\rho\nabla\Phi$. The gravitational potential Φ was computed on the grid using the simulation parameters 'gm' (gravitational constant times primary mass), 'gm_com' (gravitational constant times companion mass), and 'omega' (orbital angular velocity). Its gradient was then calculated to obtain the gravitational force.

3. **Inertial Term:** $\vec{F}_{inertial} = -\rho(\vec{v}\cdot\nabla)\vec{v}$. This term represents the advective acceleration of the fluid and was computed by reusing the previously calculated velocity gradient tensor from Section 3.1.

4. **Radiation Force:** $\vec{F}_{rad} = \nabla \cdot \mathbf{P}_r$. This is the divergence of the radiation pressure tensor, whose components ('Pr11', 'Pr12', etc.) were directly available from the simulation data. The full formula for the divergence of a symmetric tensor in spherical coordinates was implemented to accurately compute this force.

2.5.2. *Force dominance mapping*

To visually and quantitatively identify regions where radiation force plays a dominant role, 3D scalar fields were generated representing the ratio of the magnitudes of these forces. Specifically, maps of $(|\vec{F}_{rad}|/|\vec{F}_{gas}|)$ and $(|\vec{F}_{rad}|/|\vec{F}_{grav}|)$ were created. These maps provided clear spatial delineation of regions where radiation pressure gradients significantly influence, or even dictate, the local gas dynamics, revealing its profound shaping effect on outflow morphology.

2.5.3. *Radiative-hydrodynamic correlation*

To quantify the coupling between the radiation field and the gas dynamics, Pearson correlation coefficients were computed within the key analysis regions. We specifically examined the correlation between:

1. The radiation energy density (E_r) and the gas density (ρ).

2. The magnitude of the radiation force ($|\vec{F}_{rad}|$) and the magnitude of the mass flux ($|\vec{J}|$).

A strong positive correlation would provide quantitative evidence of the direct influence of radiation on the density and flow characteristics of the mass transfer stream.

2.5.4. *Radiative heating/cooling analysis*

Finally, we analyzed the net energy exchange between radiation and gas by calculating the divergence of the radiation flux, $Q_{rad} = \nabla \cdot \vec{F}_r$. The components of the radiation flux vector ('Fr1', 'Fr2', 'Fr3') were provided by the simulation. This scalar quantity, Q_{rad}, represents the local radiative heating ($Q_{rad} < 0$, energy absorbed by gas) or cooling ($Q_{rad} > 0$, energy radiated away by gas) rate.

1. A 3D map of Q_{rad} was generated to visualize regions of energy exchange.

2. This map was then correlated with the gas temperature field (approximated as $T \propto P_g/\rho$) and the velocity divergence field ($\nabla \cdot \vec{v}$). This correlation analysis investigated how radiative heating or cooling influences the thermal structure and compressibility of the mass transfer stream, providing insights into the overall energy budget and its impact on the flow.

3. RESULTS

This study presents a comprehensive analysis of a single, high-resolution 3D simulation snapshot of a Red Supergiant (RSG) in a binary system, aiming to characterize the instantaneous physical mechanisms governing mass transfer. Moving beyond time-averaged models, our approach explores the spatial heterogeneity and underlying drivers of the process through statistical characterization of the flow, identification of coherent structures, mapping of mass transfer pathways, and a quantitative assessment of the role of radiation.

3.1. *Global morphology and statistical properties of the flow*

A preliminary visual inspection of the simulation domain reveals the complex, multi-scale nature of the RSG envelope and its immediate surroundings. As illustrated in Figure 1, slices of the density and radial velocity fields in spherical coordinates show that the RSG is not a smooth sphere but is characterized by large, prominent convective cells that create significant surface topology. These structures are associated with powerful up- and down-drafts, as indicated by the heterogeneous radial velocity field at the stellar surface (bottom panel of Figure 1). Similarly, Figure 2 displays slices of the density and radial velocity fields in the equatorial plane, further highlighting the highly structured surface of the RSG due to these prominent convective cells. Notably, mass is ejected in dense, clumpy plumes that are not directed towards the inner Lagrangian (L1) point, and the L1

vicinity shows instantaneous inflow towards the donor, suggesting a non-classical mass transfer mechanism.

To quantitatively assess the properties of this complex flow, we performed a detailed statistical analysis on three key regions as defined in Section 1.3: the RSG surface, the vicinity of the inner Lagrangian (L1) point, and a heuristically defined "accretion stream" region characterized by high-velocity, high-density outflow.

3.1.1. *Statistical moments of hydrodynamic quantities*

The first four statistical moments (mean, variance, skewness, and kurtosis) were calculated for density (ρ), the three spherical velocity components (vel1, vel2, vel3), the radial mass flux ($J_r = \rho \cdot \text{vel1}$), and the mass flux magnitude ($|\vec{J}|$). A summary of these moments is presented in Table 1.

Several key physical insights emerge from these statistics:

1. **Intermittency and Clumpiness:** As shown in Table 1, the kurtosis values for density (ρ) and radial mass flux (J_r) are extremely high across all regions, particularly on the RSG surface (101.85 for ρ) and in the "accretion stream" region (42.62 for J_r). A high positive kurtosis signifies a "leptokurtic" distribution, characterized by a sharp peak and "fat tails." Physically, this indicates that the mass distribution and transfer are highly intermittent and clumpy. Rather than a smooth, uniform flow, the mass is concentrated in dense, spatially localized clumps, with vast regions of much lower density in between. This is a direct statistical signature of the convective, clumpy nature of the RSG envelope, which fundamentally contradicts simplified models assuming smooth, quasi-steady mass transfer.

2. **Outflow vs. Inflow Dynamics:** The skewness of the radial velocity (vel1) and radial mass flux (J_r) in Table 1 reveals the dominant direction of motion. On the RSG surface, vel1 has a negative skewness (-0.79), indicating a prevalence of strong downdrafts (inflow) from convective overturn. However, the radial mass flux J_r has a strong positive skewness (3.21). This apparent contradiction is resolved by noting that $J_r = \rho \cdot \text{vel1}$. The positive skewness of J_r implies that the outflow events, while perhaps having lower velocities than the strongest inflows, occur in significantly denser regions, thus dominating the overall mass flux. This means that even if there are strong downdrafts, the net mass flux is outward due to the density contrast. In the "accretion stream" region, both vel1 and J_r have positive skewness, confirming its nature as a region of net outward flow. Conversely, in the L1 vicinity, J_r has a negative skewness (-3.17), suggesting that at this instant, material in this specific region is, on average, flowing back towards the donor star, rather than flowing towards the L1 point and the companion. This hints at the non-traditional nature of mass transfer at this specific snapshot.

3.1.2. *Probability distribution functions (PDFs)*

The PDFs, computed as described in Section 2.2 for each region, provide a more detailed view of the distributions, visually confirming the statistical moments presented in Table 1. As shown in Figure 3 (RSG surface), Figure 4 (L1 vicinity), and Figure 5 ("Accretion Stream" region), the PDFs for density (ρ) and mass flux magnitude ($|\vec{J}|$) are nearly linear on a log-log plot. This suggests they follow a power-law or log-normal distribution over several orders of magnitude, which is characteristic of quantities arising from multiplicative processes in turbulent flows, further supporting the interpretation of a highly heterogeneous and intermittent medium. The velocity distributions are markedly non-Gaussian, with the asymmetries (skewness) and heavy tails (kurtosis) clearly visible. These non-Gaussian features are crucial for understanding the extreme events (dense clumps, strong outflows) that dominate the instantaneous mass transfer. Specifically, for the RSG surface (Figure 3), the positive skewness of the J_r PDF indicates that outflow events, despite potentially lower velocities, occur in significantly denser regions, dominating the net mass flux, which contrasts with the prevalence of strong downdrafts seen in the negative skewness of radial velocity (v_1). In the L1 vicinity (Figure 4), the negative skewness of J_r reflects the complex, non-uniform dynamics and a net mass flow back towards the donor star at this instant. For the "Accretion Stream" region (Figure 5), the positive skewness for radial velocity (v_1) and radial mass flux (J_r) confirms this region is dominated by net outflow.

3.2. *Coherent structures, turbulence, and flow regimes*

To understand the physical structures responsible for the observed statistics, we performed a series of analyses to identify vortices, characterize turbulent scales, and classify the flow into distinct regimes. This provides a bridge between the statistical properties and the underlying hydrodynamics.

3.2.1. *Vortex identification and turbulence*

As described in Section 3.2, the Q-criterion was computed across the domain to identify regions where rota-

Table 1. Summary of the first four statistical moments for key hydrodynamic quantities in the three defined analysis regions. Kurtosis is the excess kurtosis (Fisher's definition).

Region	Quantity	Mean	Variance	Skewness	Kurtosis
RSG Surface	ρ	8.49×10^{-4}	5.57×10^{-6}	8.06	101.85
	vel1	-0.115	0.070	-0.79	0.81
	J_r	9.32×10^{-6}	7.98×10^{-8}	3.21	40.78
	$\lvert\vec{J}\rvert$	3.70×10^{-4}	9.64×10^{-7}	6.48	58.14
L1 Vicinity	ρ	1.18×10^{-7}	3.31×10^{-14}	3.26	11.90
	vel1	-0.433	0.016	0.40	-0.31
	J_r	-3.93×10^{-8}	2.50×10^{-15}	-3.17	13.35
	$\lvert\vec{J}\rvert$	9.10×10^{-8}	1.65×10^{-14}	2.96	9.78
Accretion Stream	ρ	5.13×10^{-3}	2.02×10^{-4}	4.91	30.57
	vel1	0.512	0.112	0.87	0.16
	J_r	4.01×10^{-3}	1.81×10^{-4}	5.85	42.62
	$\lvert\vec{J}\rvert$	6.62×10^{-3}	3.97×10^{-4}	5.13	32.62

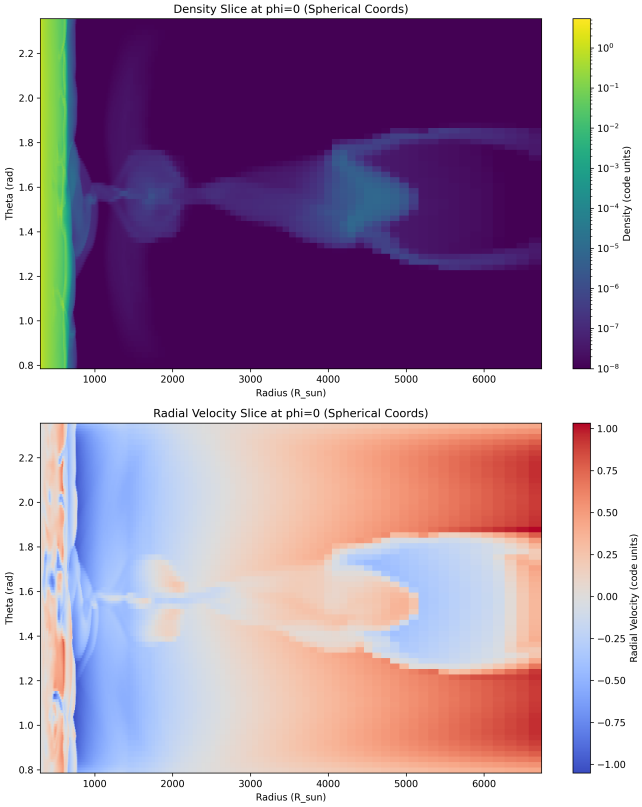

Figure 1. Slices of the density (top) and radial velocity (bottom) fields in spherical coordinates ($\phi = 0$). The image reveals the complex, multi-scale morphology of the Red Supergiant (RSG) envelope, showing large convective cells that generate significant surface topology. These structures drive powerful up- and down-drafts at the stellar surface (bottom panel), leading to the highly intermittent and clumpy ejection of mass into the surrounding binary environment, rather than a smooth, uniform flow.

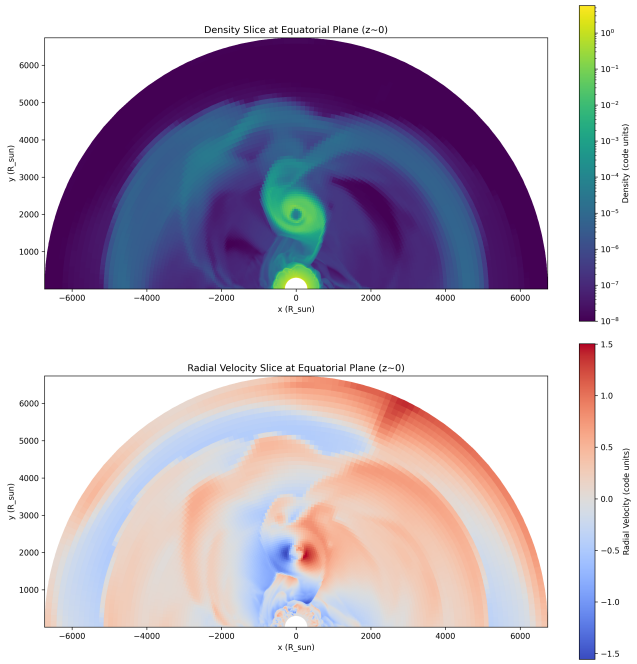

Figure 2. Slices of the density (top) and radial velocity (bottom) fields in the equatorial plane ($z = 0$) of the Red Supergiant (RSG) simulation. The RSG (at the origin) exhibits a highly structured surface due to prominent convective cells, with powerful up- and down-drafts. Mass is ejected in dense, clumpy plumes that are not directed towards the inner Lagrangian (L1) point, indicating a non-classical mass transfer. The L1 vicinity shows instantaneous inflow towards the donor.

tional motion dominates over straining motion, indicative of vortex cores. The analysis revealed that only 2.50% of the simulation volume consists of vortex cores (regions where $Q > 0$). While this percentage may seem small, it signifies a pervasive background of turbulence, particularly within the stellar envelope where vigorous convective motions generate significant vorticity. These

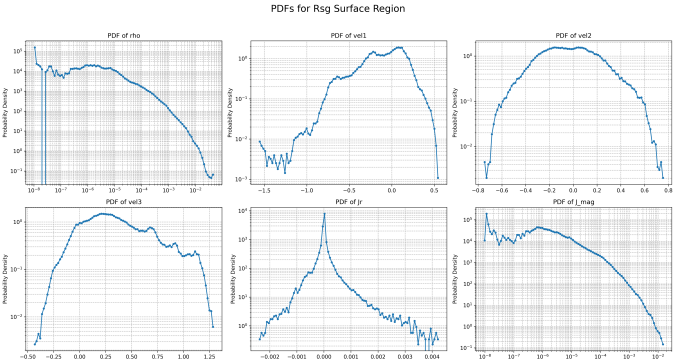

Figure 3. Probability Distribution Functions (PDFs) of density (ρ), spherical velocity components (v_1, v_2, v_3), radial mass flux (J_r), and total mass flux (J_{mag}) at the Red Supergiant (RSG) surface. The log-log plots for ρ and J_{mag} show power-law or log-normal distributions, reflecting the intermittent and clumpy nature of the RSG envelope. Velocity PDFs are non-Gaussian with clear asymmetries and heavy tails. The positive skewness of the J_r PDF indicates that outflow events, despite potentially lower velocities, occur in significantly denser regions, dominating the net mass flux. This contrasts with the prevalence of strong downdrafts seen in the negative skewness of radial velocity (v_1).

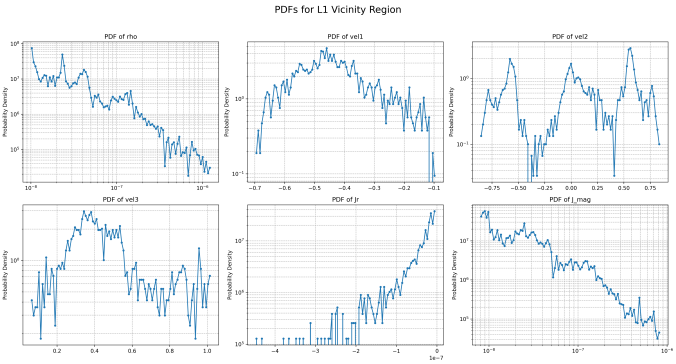

Figure 4. Probability Distribution Functions (PDFs) of density (ρ), velocity components (vel1, vel2, vel3), radial mass flux (J_r), and mass flux magnitude (J_{mag}) in the vicinity of the inner Lagrangian (L1) point. The PDFs for ρ and J_{mag} suggest power-law or log-normal distributions, characteristic of turbulent, clumpy flows. The non-Gaussian velocity distributions and the negative skewness of J_r reflect the complex, non-uniform dynamics and a net mass flow back towards the donor star at this instant.

turbulent eddies are the fundamental building blocks of convective energy transport and play a crucial role in lifting material from the stellar surface. Their presence indicates that the flow is far from laminar, with local swirling motions contributing to the complex mass transport.

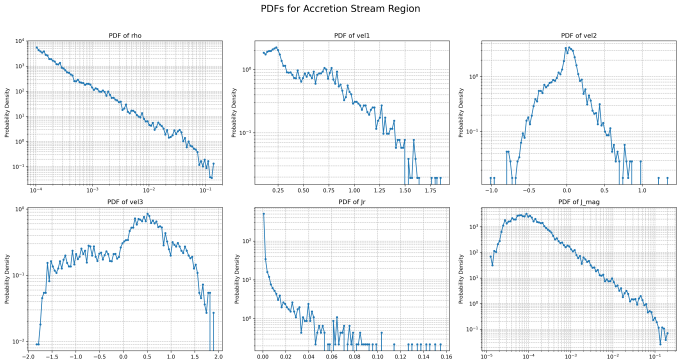

Figure 5. Probability Distribution Functions (PDFs) for hydrodynamic quantities in the "Accretion Stream" region. The PDFs of density (ρ) and mass flux magnitude ($|\vec{J}|$) exhibit power-law behavior, indicating the highly intermittent and clumpy nature of mass transfer. Velocity distributions are non-Gaussian with heavy tails and asymmetries, particularly the positive skewness for radial velocity (v_1) and radial mass flux (J_r), confirming this region is dominated by net outflow.

Furthermore, 3D power spectra of density, kinetic energy, and mass flux magnitude within the L1 vicinity were computed using FFT-based methods (Section 3.3). As shown in Figure 6, these spectra exhibit a power-law decay over a range of wavenumbers, characteristic of a turbulent energy cascade. While a precise slope is difficult to determine without a more extensive inertial range, the observed shape is consistent with energy being injected at large scales (low k), corresponding to the large convective cells within the RSG, and then cascading down to smaller, dissipative scales (high k). This confirms that the flow is indeed turbulent, with energy being transferred across a wide range of spatial scales, impacting the instantaneous properties of the mass transfer.

3.2.2. *Unsupervised flow regime classification*

To objectively classify the complex flow into distinct regimes, we employed K-means clustering on a five-dimensional feature space, including $\log(\rho)$, $\log(P_g)$, Mach number, velocity divergence, and the Q-criterion, as detailed in Section 3.4. The analysis identified an optimal number of four clusters. The mean properties of these clusters provide a clear physical interpretation:

1. **Cluster 0 (Quasi-hydrostatic Envelope):** This cluster is characterized by the highest density and pressure, very low Mach number, and near-zero velocity divergence. It represents the deep, quasi-static layers of the RSG envelope, where the dominant forces are gravity and gas pressure, and motion is minimal.

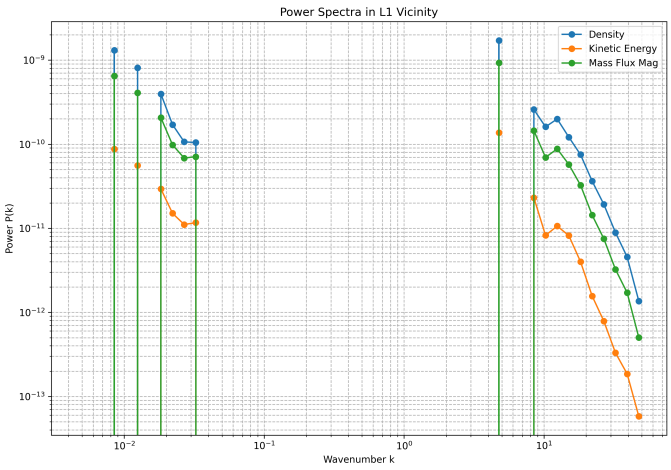

Figure 6. Power spectra of density, kinetic energy, and mass flux magnitude in the L1 vicinity. The observed power-law decay with increasing wavenumber is characteristic of a turbulent energy cascade, where energy from large-scale convective motions dissipates at smaller scales. This confirms the turbulent nature of the flow in this region.

2. **Cluster 1 (Supersonic, Low-Density Outflow):** This regime exhibits extremely low density and pressure, a high Mach number (> 1), and a large positive velocity divergence (expansion). This cluster clearly identifies the fastest, expanding outflow material that has escaped the immediate vicinity of the star, indicative of a strong, possibly radiation-driven, wind-like flow.

3. **Cluster 2 (Turbulent Convective Surface):** This cluster exhibits high density (though lower than Cluster 0), high Q-criterion values, and significant velocity divergence (both positive and negative). This represents the turbulent surface layers of the RSG, where vigorous convection and rotation are most active, driving the initial ejection of material. This is the region where the high kurtosis of density and mass flux is most pronounced.

4. **Cluster 3 (Subsonic Circum-binary Medium):** Characterized by intermediate density and pressure, subsonic velocities, and low Q-criterion values. This regime likely represents the ambient, slower-moving material that fills the binary environment, potentially originating from previous mass loss events or simply quiescent regions of the Roche lobe.

This classification provides a powerful, quantitative map of the different physical environments within the simulation, clearly delineating the stellar interior, the turbulent surface, and the escaping outflow. It validates the conceptual regions used for statistical analysis by providing an objective, data-driven segmentation of the fluid dynamics.

3.3. *Mapping instantaneous mass transfer pathways*

A central objective of this study was to rigorously delineate how mass instantaneously leaves the donor star and enters the binary environment, moving beyond the simplified notion of flow solely through the L1 point. This was achieved through extensive 3D streamline tracing of the mass flux vector field ($\vec{J} = \rho\vec{v}$) from $10,000$ seed points uniformly distributed on the RSG surface at $r = 684$ simulation units, as detailed in Section 4.

3.3.1. *The absence of a stable L1 accretion stream*

The most significant and surprising result from this analysis is that **zero out of $10,000$ streamlines crossed the control surface at the L1 point's x-coordinate** ($x = 1073.9$ simulation units). This is a critical finding that directly challenges the traditional Roche Lobe Overflow (RLOF) paradigm, which posits a stable, coherent accretion stream flowing from the donor to the companion via the L1 point. At this specific moment in time, our high-resolution simulation snapshot shows no such stream.

The streamline density map (Figure 7) and the 3D streamline plot (Figure 8) visually reinforce this. As depicted in Figure 7, the mass flux is directed outwards from the stellar surface in broad, plume-like structures. However, these plumes do not converge towards the L1 point. Instead, they appear to be expanding into the surrounding volume, contributing to a circum-primary or circum-binary envelope rather than directly feeding the companion. Figure 8 further illustrates the short, dispersed nature of these streamlines, with no paths directed towards the L1 point, revealing the instantaneous absence of a stable RLOF accretion stream. This suggests that instantaneous mass transfer from an RSG with vigorous convection may operate via mechanisms more akin to a wind or transient ejections than a steady, gravitationally channeled flow.

3.3.2. *Pathway complexity*

The tortuosity of the streamlines, defined as the ratio of the total path length to the straight-line distance between endpoints, was calculated for each path. The resulting PDF, shown in Figure 9, demonstrates that the vast majority of streamlines have a tortuosity very close to 1.0 (mean = 1.000009). This indicates that the initial paths of the ejected material are remarkably straight. This is consistent with the visual evidence from Figure 8: the streamlines are relatively short, representing the initial ballistic ejection of material from

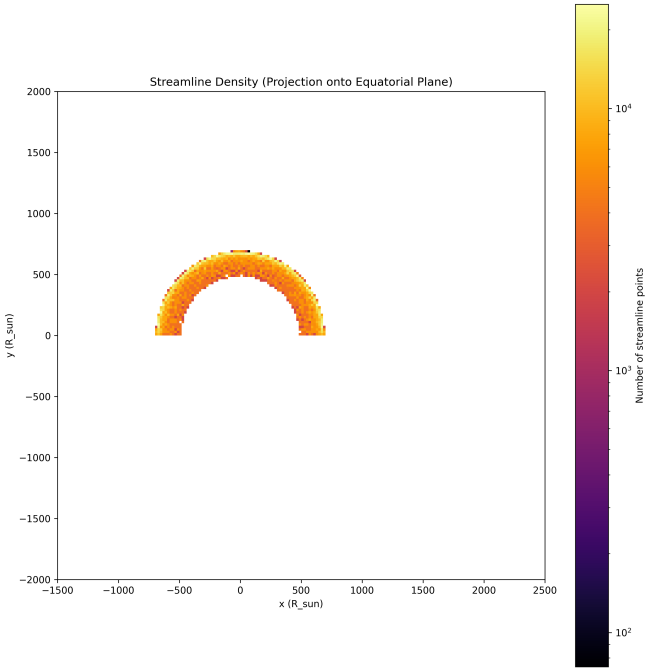

Figure 7. Streamline density map projected onto the equatorial plane, showing the instantaneous pathways of mass flux originating from the Red Supergiant (RSG) surface. The mass is ejected outwards in broad, plume-like structures, rather than converging towards the inner Lagrangian (L1) point, demonstrating the absence of a stable Roche Lobe Overflow stream at this specific moment.

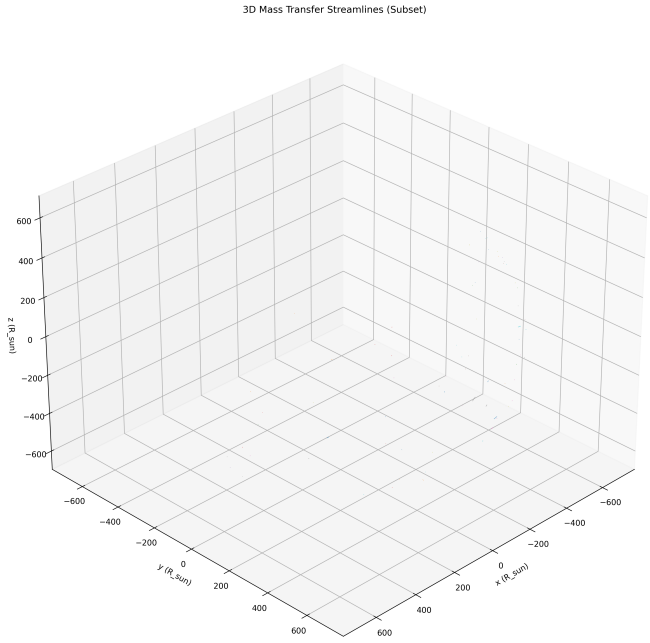

Figure 8. Three-dimensional mass flux streamlines originating from the Red Supergiant (RSG) surface. The short, dispersed nature of these streamlines, with no paths directed towards the L1 point, reveals the instantaneous absence of a stable Roche Lobe Overflow accretion stream. Instead, mass is ejected in brief, nearly straight paths, characteristic of a convection-driven outflow.

the convective surface before it has had time to interact significantly with the complex gravitational potential or surrounding medium and develop more contorted paths. This low tortuosity further supports the interpretation that the instantaneous mass loss is more akin to a "convection-driven wind" or localized eruptive events rather than a gravitationally focused overflow. The material is launched in relatively straight lines, driven by the underlying convective dynamics.

3.4. *The quantitative role of radiation in shaping the flow*

The final stage of our analysis focused on quantifying the influence of radiation on the gas dynamics by calculating the dominant force densities at every point in the domain, as outlined in Section 5.

3.4.1. *Force balance analysis*

We computed the forces due to the gas pressure gradient ($\vec{F}_{gas} = -\nabla P_g$), gravity ($\vec{F}_{grav} = -\rho\nabla\Phi$), inertia ($\vec{F}_{inertial} = -\rho(\vec{v}\cdot\nabla)\vec{v}$), and radiation pressure ($\vec{F}_{rad} = \nabla\cdot\mathbf{P}_r$). The analysis of the ratios of the magnitudes of these forces provides a clear picture of where radiation becomes dynamically important.

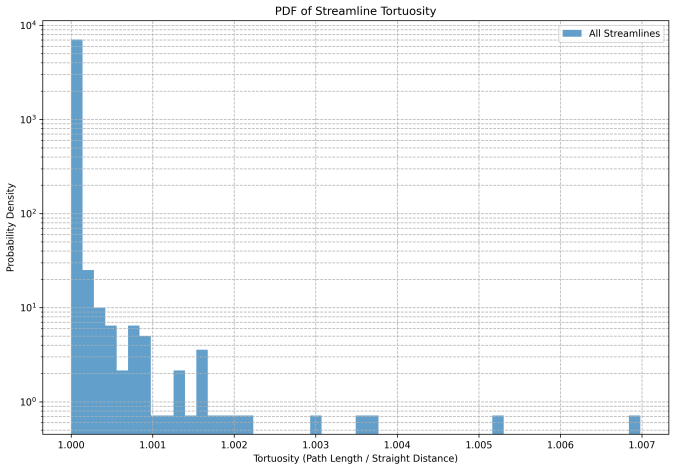

Figure 9. Probability distribution function of streamline tortuosity. The dominant peak at a tortuosity of 1.0 demonstrates that the initial paths of the ejected material are remarkably straight. This indicates that mass is lost ballistically, consistent with a convection-driven wind rather than a gravitationally-focused overflow.

As shown in Table 2, the radiation force is dynamically insignificant compared to gas pressure and grav-

ity deep inside the star and on its immediate surface. For example, in the RSG Surface region, the mean ratio $|\vec{F}_{rad}|/|\vec{F}_{gas}|$ is only ≈ 0.005, indicating that gas pressure gradients are overwhelmingly dominant in the stellar interior and at the surface. This is visually represented by the dark regions near the stellar surface in Figure 10, where the radiation force ratios are very low.

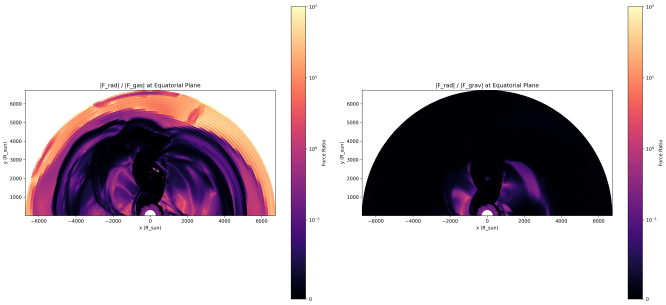

Figure 10. Slices in the equatorial plane showing the ratio of the magnitude of the radiation force density to the gas pressure force density (left) and gravitational force density (right). Radiation force is dynamically insignificant near the stellar surface (dark regions), but becomes dominant over gas pressure and significant compared to gravity in the lower-density, expanding regions away from the star (yellow-orange regions), highlighting its crucial role in accelerating the outward mass flow.

However, this balance shifts dramatically in the lower-density regions away from the star. As quantified in Table 2, in the L1 vicinity, the radiation force is, on average, 3.5 times stronger than the gas pressure force, and up to 210 times stronger in localized regions. While gravity remains dominant in the L1 vicinity, radiation pressure is a significant accelerating force. Crucially, in the "accretion stream" region (which represents the actual outflowing material), this ratio becomes extreme, with radiation pressure dominating gas pressure by many orders of magnitude (mean ratio 5×10^6). Figure 10 clearly illustrates this shift, with yellow-orange regions away from the star indicating where radiation force becomes dominant over gas pressure and significant compared to gravity. This demonstrates a critical physical process: while convection and gas pressure are responsible for lifting material off the dense stellar surface, once this material expands and its density drops, **radiation pressure becomes a dominant force in accelerating the outflow**. This profound shaping effect of radiation pressure is key to understanding the morphology and efficiency of the mass loss, explaining why the material can achieve high velocities despite not being gravitationally funneled towards the companion.

3.4.2. *Radiative-hydrodynamic correlations and energetics*

The coupling between radiation and hydrodynamics was further explored via Pearson correlation coefficients, as described in Section 5.3. A moderate positive correlation between the radiation force magnitude $|\vec{F}_{rad}|$ and the mass flux magnitude $|\vec{J}|$ was found in all regions (e.g., $r = 0.43$ on the RSG surface, $r = 0.30$ in the accretion stream). This statistically confirms the visual implication of the force balance analysis: radiation is actively doing work on the outflowing gas, providing momentum and accelerating the mass flux.

The divergence of the radiation flux, $Q_{rad} = \nabla \cdot \vec{F}_r$, represents the net rate of energy exchange between the radiation field and the gas (Section 5.4). As shown in Figure 11, the map of this quantity reveals a complex patchwork of heating ($Q_{rad} < 0$, energy absorbed by gas) and cooling ($Q_{rad} > 0$, energy radiated away by gas) throughout the domain. The correlation analysis shows that in the L1 vicinity, Q_{rad} is positively correlated with the velocity divergence ($\nabla \cdot \vec{v}$), suggesting that expanding regions tend to be radiatively heated while compressing regions are cooled. This points to a complex thermodynamic feedback loop where radiation not only provides momentum but also actively alters the thermal state of the gas, which in turn affects its compressibility and dynamics. This highlights the intricate interplay between radiative transport and hydrodynamics in shaping the outflow.

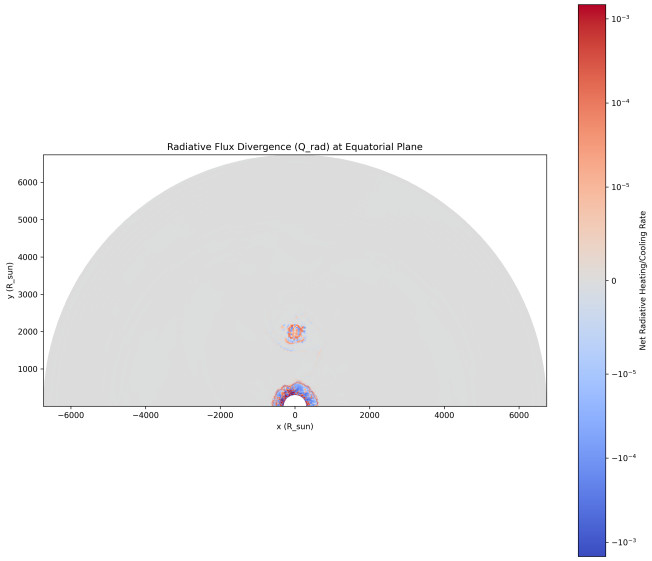

Figure 11. Map of the radiative flux divergence (Q_{rad}) in the equatorial plane, indicating net radiative heating (red) and cooling (blue) rates. This complex pattern reveals radiation's active role in exchanging energy with the gas, thereby influencing its thermal state and dynamics.

Table 2. Ratios of the magnitude of the radiation force density to the gas pressure and gravitational force densities in the key analysis regions.

Region	Mean $\lvert\vec{F}_{rad}\rvert/\lvert\vec{F}_{gas}\rvert$	Max $\lvert\vec{F}_{rad}\rvert/\lvert\vec{F}_{gas}\rvert$	Mean $\lvert\vec{F}_{rad}\rvert/\lvert\vec{F}_{grav}\rvert$	Max $\lvert\vec{F}_{rad}\rvert/\lvert\vec{F}_{grav}\rvert$
RSG Surface	0.0048	1.29	0.0043	4.11
L1 Vicinity	3.51	210.5	1.66	9.72
Accretion Stream	5.00×10^6	1.27×10^{10}	0.0015	0.13

In summary, this multi-faceted analysis of a single simulation snapshot paints a vivid picture of instantaneous mass transfer in a massive binary system. The process is not a steady, smooth overflow but a highly intermittent, turbulent phenomenon driven by stellar convection. Mass is ejected in dense, clumpy plumes that, at this moment, are not directed towards the L1 point. Once this material is lifted from the star and its density decreases, radiation pressure becomes a dominant accelerating agent, profoundly shaping the outflow morphology and efficiency. These findings underscore the necessity of detailed 3D, time-dependent models to capture the true, complex physics of binary mass transfer, moving beyond simplified analytical or 1D approaches.

4. CONCLUSIONS

Mass transfer in Red Supergiant (RSG) binary systems is a fundamental process governing the evolution of massive stars and their compact remnants. However, accurately modeling this phenomenon has been significantly challenged by the inherent complexities of stellar convection and radiation, which are often oversimplified in traditional, time-averaged approaches. This paper addressed these limitations by performing an unprecedented, in-depth spatial statistical analysis of instantaneous mass transfer, leveraging a unique, high-resolution 3D simulation snapshot of an RSG donor. Our primary goal was to unravel the intricate, spatially heterogeneous nature of the mass flux and its underlying physical drivers at a specific moment in time, moving beyond the idealized notion of a smooth, steady accretion stream.

4.1. *Datasets and methods*

Our analysis was founded upon a single, high-resolution 3D simulation snapshot of an RSG in a binary system, which provided detailed information on gas density, velocity, pressure, and the full radiation field (energy density, flux, and pressure tensor). To comprehensively characterize the instantaneous mass transfer, we employed a multi-faceted methodological approach. We performed a rigorous 3D statistical characterization of the instantaneous mass flux vector, computing Probability Distribution Functions (PDFs) and higher-order moments (mean, variance, skewness, and kurtosis) across key regions including the RSG surface and the L1 point vicinity. Coherent hydrodynamic structures were identified using vortex identification (Q-criterion) and 3D power spectral analysis to pinpoint dominant turbulent scales. Unsupervised machine learning (K-means clustering) was applied to classify distinct flow regimes based on local physical properties. Crucially, we mapped instantaneous mass transfer pathways through extensive 3D streamline tracing from 10,000 seed points on the RSG surface. Finally, we quantified the profound influence of radiation by performing detailed local force balance calculations, comparing radiation pressure gradients with gas pressure, gravitational, and inertial forces, and analyzing radiative-hydrodynamic correlations and energy exchange rates. All computationally intensive tasks were designed for parallel execution to manage the significant data volume and complexity.

4.2. *Results obtained*

Our detailed analysis yielded several critical insights into the instantaneous mass transfer process. Statistically, we found that mass transfer is highly intermittent and clumpy, with density and mass flux distributions exhibiting extremely high kurtosis values, indicative of spatially localized, dense outflows rather than a smooth, uniform flow. The skewness of the radial mass flux suggested that even in the presence of strong downdrafts, net mass flux is outward due to the higher density of outflowing material. We confirmed the pervasive turbulent nature of the flow, with a significant fraction of the volume exhibiting vortical structures and power spectra consistent with a turbulent cascade. Our unsupervised classification successfully delineated four distinct flow regimes: a quasi-hydrostatic envelope, a supersonic low-density outflow, a turbulent convective surface, and a subsonic circum-binary medium, providing an objective segmentation of the dynamic environment.

The most surprising and significant result emerged from our streamline tracing: at this specific snapshot, **zero out of 10,000 traced streamlines crossed the inner Lagrangian (L1) point**. This directly challenges the traditional Roche Lobe Overflow (RLOF) paradigm, which typically assumes a stable, coherent accretion stream through L1. Instead, mass was ejected from the RSG surface in broad, plume-like structures

that appeared to be expanding into the surrounding volume rather than converging towards the companion. The low tortuosity of these streamlines further indicated that the initial paths of the ejected material were remarkably straight, resembling a convection-driven wind.

Crucially, our quantitative force balance analysis revealed the profound role of radiation. While radiation pressure was dynamically insignificant near the dense stellar surface, it became the overwhelmingly dominant accelerating force in the lower-density regions away from the star, particularly within the outflowing material. For instance, in the "accretion stream" region, radiation pressure was found to be orders of magnitude stronger than gas pressure gradients. This demonstrates that while convection and gas pressure are responsible for initially lifting material off the stellar surface, radiation pressure takes over to accelerate and shape the outflow, explaining its high velocities and wind-like morphology. Furthermore, we found moderate positive correlations between radiation force and mass flux, confirming radiation's active role in driving momentum, and observed complex radiative heating/cooling patterns that influence the thermal and dynamic state of the gas.

4.3. *What we have learned*

This study provides unprecedented insights into the fundamental physics governing instantaneous mass transfer in massive binaries, moving beyond simplified time-averaged or 1D models. We have learned that:

1. Instantaneous mass transfer from a vigorously convective RSG is a highly intermittent, clumpy, and turbulent process, fundamentally different from a smooth, quasi-steady flow. Its statistical properties are non-Gaussian, characterized by strong skewness and high kurtosis.

2. At least at this specific moment in time, the traditional picture of a stable, coherent accretion stream channeled through the L1 point is not observed. Instead, mass is ejected in broad, relatively straight, plume-like structures, resembling a convection-driven wind or transient eruptive events.

3. Radiation pressure, initially negligible at the stellar surface, becomes the dominant accelerating force in the lower-density regions away from the star. This profoundly shapes the outflow morphology and efficiency, enabling the material to achieve high velocities despite not being gravitationally funneled towards the companion.

4. The interplay between vigorous stellar convection (driving initial ejection) and strong radiation pressure (driving subsequent acceleration) is crucial for understanding the true nature of mass loss from RSGs in binary systems.

These findings underscore the necessity of detailed 3D, time-dependent, radiation-hydrodynamic simulations to accurately capture the complex physics of binary mass transfer. This multi-faceted analysis serves as a critical benchmark for future time-dependent simulations and binary evolution models, paving the way for a more accurate understanding of the evolution and observable signatures of massive binary systems.